Exact parameter relations and effective masses within sp^3 zinc-blende tight-binding models

J. P. Loehr
Avionics Directorate (WL/AADP), Wright Patterson Air Force Base, Ohio 45433-6543

D. N. Talwar
Department of Physics, Indiana University of Pennsylvania, Indiana, Pennsylvania 15705-1087

(Received 17 September 1996)

Working within the next-nearest-neighbor sp^3 zinc-blende model, we restrict the number of free tight-binding parameters from 23 to 8 by directly inverting the Γ-, X-, and L-point energy expressions. In addition, we solve for the parameter dependence of the (001) conduction- and valence-band masses and present optimized parameter sets for GaAs, GaSb, AlAs, InAs, and InSb. The optimal parameters are incorporated in energy-gap calculations for InAs/$In_xGa_{1-x}Sb$ superlattices. [S0163-1829(97)07607-8]

I. INTRODUCTION

Until fast first-principles band-structure algorithms emerge providing energies and wave functions accurate enough for semiconductor device calculations, we must resort to semiempirical models such as tight binding[1–3] or $\mathbf{k}\cdot\mathbf{p}$.[4,5] In these approaches we model the Hamiltonian matrix by introducing some set of unknown parameters, diagonalize the matrix at various critical points or along particular directions, and selectively compare the results with experimental data to determine *constraint equations* for the empirical parameters. Naturally there is an inherent trade-off between model complexity—measured by the number of parameters and the dimension of the Hamiltonian matrix—and the number of constraints that can be satisfied. For quantum-well and superlattice device calculations[6–9] it is most important to reproduce the zone-center carrier masses and band gaps and to address real-space effects such as electric fields, strain, and interface bonding. The tight-binding and $\mathbf{k}\cdot\mathbf{p}$ models complement each other in treating these problems.

In $\mathbf{k}\cdot\mathbf{p}$ models the carrier masses are simple functions of the empirical parameters, spin-orbit effects are relatively easy to incorporate, and closed-form expressions exist for all parameters. But the models are only valid near the zone center—compromising their accuracy when applied to short-period superlattices—and, in most incarnations, include only the fcc *lattice* symmetry and cannot reveal the richer zinc-blende *crystal* structure. Tight-binding models, by contrast, embed the full zinc-blende lattice symmetry in the solutions and are valid throughout the Brillouin zone. The constraint equations relating the band energies at Γ, X, and L to the overlap integrals take a simple form, but heretofore they have not been inverted. If spin-orbit effects are introduced, in order to accurately describe the valence band, the constraint equations become more complicated. Perhaps the greatest impediment to successful tight-binding device calculations is that in all models the zone-center electron and hole *masses* are complicated functions of the empirical parameters. Consequently, the overlap integrals are often determined by *ad hoc* numerical fitting and the carrier masses are rarely correct.[10]

In this paper we invert the constraint equations for the spinless sp^3 zinc-blende next-nearest-neighbor tight-binding model and derive the exact dependence of the (001) zone-center conduction- and valence-band masses on the tight-binding parameters. This allows us to reduce the number of independent empirical parameters from 23 to 8, and we exploit the reduction to optimize the tight-binding parameters for many III-V compounds. The new parameters reproduce the electron and heavy-hole masses, as well as the critical point energies at the Γ, X, and L points. We incorporate these parameters in band-gap calculations for InAs/$In_xGa_{1-x}Sb$ superlattices.

II. FITTING PROCEDURE

A. Critical point energies

Notations for the critical points, definitions of the empirical parameters, and matrix elements of the tight-binding Hamiltonian have been given previously in Ref. 11, subject to the corrections in our Appendix. Closed-form expressions for many Γ, X, and L energies also have been given and are repeated below for convenience:

$$E(\Gamma_{1v}^{c}) = \tfrac{1}{2}(A+B) \pm \sqrt{[(A-B)/2]^2 + P_5^2}, \tag{1}$$

$$E(\Gamma_{15v}^{c}) = \tfrac{1}{2}(C+D) \pm \sqrt{[(C-D)/2]^2 + P_8^2}, \tag{2}$$

$$E(X_{3v}^{c}) = \tfrac{1}{2}(E+F) \pm \sqrt{[(E-F)/2]^2 + P_7^2}, \tag{3}$$

$$E(X_{1v}^{c}) = \tfrac{1}{2}(G+H) \pm \sqrt{[(G-H)/2]^2 + P_6^2}, \tag{4}$$

$$E(X_{5v}^{c}) = \tfrac{1}{2}(I+J) \pm \sqrt{[(I-J)/2]^2 + P_9^2}, \tag{5}$$

$$E(L_{3v}^{c}) = \tfrac{1}{2}(K+L) \pm \sqrt{[(K-L)/2]^2 + [(P_8+P_9)/2]^2}. \tag{6}$$

Here the upper (lower) sign is for the conduction- (valence-) band states and the abbreviations $A-L$ are *defined* in terms of the overlap integrals as

$$A \equiv P_1 + 3P_{18}, \quad B \equiv P_2 + 3P_{19}, \tag{7}$$

$$C \equiv P_3 + 2P_{14} + P_{10}, \quad D \equiv P_4 + 2P_{15} + P_{11}, \tag{8}$$

$$E \equiv P_2 - P_{19}, \quad F \equiv P_3 - 2P_{14} + P_{10}, \tag{9}$$

$$G \equiv P_1 - P_{18}, \quad H \equiv P_4 - 2P_{15} + P_{11}, \tag{10}$$

$$I \equiv P_3 - P_{10}, \quad J \equiv P_4 - P_{11}, \tag{11}$$

$$K \equiv P_3 + P_{12}, \quad L \equiv P_4 + P_{13}. \tag{12}$$

The remaining L-point energies $E(L_{1v})$, $E(L_{2v})$, $E(L_{1c})$, and $E(L_{2c})$ are the eigenvalues of the matrix

$$\begin{bmatrix} P_1 & \frac{1}{2\sqrt{2}}(1-i)P_5 & -\sqrt{3}P_{20} & -\frac{\sqrt{3}}{2\sqrt{2}}(1-i)P_6 \\ \frac{1}{2\sqrt{2}}(1+i)P_5 & P_2 & \frac{\sqrt{3}}{2\sqrt{2}}(1+i)P_7 & \sqrt{3}P_{21} \\ -\sqrt{3}P_{20} & -\frac{\sqrt{3}}{2\sqrt{2}}(1-i)P_7 & P_3 - 2P_{12} & \frac{1}{2\sqrt{2}}(1+i)(P_8 - 2P_9) \\ \frac{\sqrt{3}}{2\sqrt{2}}(1+i)P_6 & \sqrt{3}P_{21} & \frac{1}{2\sqrt{2}}(1-i)(P_8 - 2P_9) & P_4 - 2P_{13} \end{bmatrix} \tag{13}$$

and cannot be expressed in closed form.

Equations (1)–(6) contain the essential physics of the tight-binding model. Most of these energy assignments are forced by the band ordering and degeneracy, but $E(X_{1v}^{c})$ and $E(X_{3v}^{c})$ are not. Our semiarbitrary choices in Eqs. (3) and (4) (which are consistent with previous calculations[2,3]) force the lower energy $E(X_{1v})$ to depend on $P_6 \equiv 4E_{sx}(0.5, 0.5, 0.5)_{01}$ and the upper energy $E(X_{3v})$ to depend on $P_7 \equiv 4E_{sx}(0.5, 0.5, 0.5)_{10}$. In diamond structures these energies are degenerate, but in zinc-blende structures the difference between the anion and cation potential breaks this symmetry. All other expressions (1), (2), (5), and (6) are symmetric with respect to the anions and cations.

After settling on Eqs. (1)–(6) we can pairwise invert them to determine A–L *solely* in terms of the experimental band energies and the driving parameters P_5–P_9. The results are

$$A = \Sigma\Gamma_1 \mp \sqrt{\Delta\Gamma_1^2 - P_5^2}, \quad B = \Sigma\Gamma_1 \pm \sqrt{\Delta\Gamma_1^2 - P_5^2}, \tag{14}$$

$$C = \Sigma\Gamma_{15} \mp \sqrt{\Delta\Gamma_{15}^2 - P_8^2}, \quad D = \Sigma\Gamma_{15} \pm \sqrt{\Delta\Gamma_{15}^2 - P_8^2}, \tag{15}$$

$$E = \Sigma X_3 \mp \sqrt{\Delta X_3^2 - P_7^2}, \quad F = \Sigma X_3 \pm \sqrt{\Delta X_3^2 - P_7^2}, \tag{16}$$

$$G = \Sigma X_1 \mp \sqrt{\Delta X_1^2 - P_6^2}, \quad H = \Sigma X_1 \pm \sqrt{\Delta X_1^2 - P_6^2}, \tag{17}$$

$$I = \Sigma X_5 \mp \sqrt{\Delta X_5^2 - P_9^2}, \quad J = \Sigma X_5 \pm \sqrt{\Delta X_5^2 - P_9^2}, \tag{18}$$

$$K = \Sigma L_3 \mp \sqrt{\Delta L_3^2 - \left(\frac{P_8 + P_9}{2}\right)^2},$$

$$L = \Sigma L_3 \pm \sqrt{\Delta L_3^2 - \left(\frac{P_8 + P_9}{2}\right)^2}, \tag{19}$$

where we have introduced the notation

$$\Sigma\Gamma_1 \equiv \tfrac{1}{2}[E(\Gamma_{1c}) + E(\Gamma_{1v})], \quad \Delta\Gamma_1 \equiv \tfrac{1}{2}[E(\Gamma_{1c}) - E(\Gamma_{1v})], \tag{20}$$

$$\Sigma\Gamma_{15} \equiv \tfrac{1}{2}[E(\Gamma_{15c}) + E(\Gamma_{15v})], \quad \Delta\Gamma_{15} \equiv \tfrac{1}{2}[E(\Gamma_{15c}) - E(\Gamma_{15v})], \tag{21}$$

$$\vdots \tag{22}$$

$$\Sigma L_3 \equiv \tfrac{1}{2}[E(L_{3c}) + E(L_{3v})], \quad \Delta L_3 \equiv \tfrac{1}{2}[E(L_{3c}) - E(L_{3v})]. \tag{23}$$

In Eqs. (14)–(19) we are forced to break the symmetry between anions and cations by choosing *signs* in each equation pair and therefore consigning $A < B$ or $B < A$, etc.; we choose the upper signs for all pairs. Although a few other sign choices give reasonable bands, most give nonsensical results.

Once A–L are fixed by P_5–P_9 and the critical point energies, it is simple to invert Eqs. (7)–(12) to determine P_1–P_4, P_{10}–P_{15}, P_{18}, and P_{19} solely in terms of empirical data and the driving parameters P_5–P_9. Thus we set

$$P_1 = (A + 3G)/4, \quad P_2 = (B + 3E)/4, \tag{24}$$

$$P_3 = (C + F + 2I)/4, \quad P_4 = (D + H + 2J)/4, \tag{25}$$

$$P_{10} = (C + F - 2I)/4, \quad P_{11} = (D + H - 2J)/4, \tag{26}$$

$$P_{12} = -(C + F + 2I - 4K)/4, \quad P_{13} = -(D + H + 2J - 4L)/4, \tag{27}$$

$$P_{14} = (C - F)/4, \quad P_{15} = (D - H)/4, \tag{28}$$

$$P_{18} = (A - G)/4, \quad P_{19} = (B - E)/4 \tag{29}$$

and immediately reduce the model from 23 to 11 empirical parameters. It is important to remember that Eqs. (7)–(12) and (24)–(29) contain no physics: they are purely notational.

B. (001) effective masses

To fit the (001) effective masses we must analytically diagonalize the Hamiltonian in a neighborhood of Γ and differentiate twice with respect to k_z to get the curvature. Upon

examining the Hamiltonian matrix along the (001) direction, where $\mathbf{k}=(0,0,k_z)$, we find that it splits into two 4×4 blocks. One block couples the $|s_0\rangle$, $|s_1\rangle$, $|p_{z0}\rangle$, and $|p_{z1}\rangle$ states and yields nondegenerate eigenvalues for all k_z. Therefore, this block gives the four nondegenerate bands: the lower Γ_{15v} band, the lower Γ_{15c} band, the Γ_{1v} band, and the Γ_{1c} (conduction) band; we fit the zone-center (001) curvature of the Γ_{1c} band to the electron effective mass. The other 4×4 block couples the $|p_{x0}\rangle$, $|p_{x1}\rangle$, $|p_{y0}\rangle$, and $|p_{y1}\rangle$ states and gives doubly degenerate eigenvalues for all k_z. Therefore these energies correspond to the two doubly degenerate bands: the upper Γ_{15c} band and the upper Γ_{15v} band. Since the model omits spin-orbit effects the Γ_{15v} band does not split into heavy-, light-, and split-off-hole states. Instead all three valence bands are degenerate at Γ, and as we move in $\mathbf{k}$ space from Γ to X these split into a nondegenerate Γ_{15v} lower band and a doubly degenerate Γ_{15v} upper band. (If spin-orbit coupling were included the upper Γ_{15v} band would break degeneracy away from Γ and split into heavy- and light-hole states.) But we can only fit our doubly degenerate Γ_{15v} band to *one* curvature at Γ, and since the heavy-hole band is typically the highest-energy band in device structures we fit this upper valence band to match the (001) heavy-hole mass.

It is difficult to obtain the conduction-band dispersion analytically since the fourth-order characteristic polynomial for the $|s_0\rangle$, $|s_1\rangle$, $|p_{z0}\rangle$, and $|p_{z1}\rangle$ block does not factor. Therefore, we calculate the conduction-band structure near Γ_{1c} to second order in k_z by perturbation theory. The calculation is somewhat tedious, requiring a basis change to first diagonalize the block at Γ, and after differentiating the second-order dispersion we obtain

$$\begin{aligned}\frac{4\hbar^2}{a_0^2 m_c^{(001)}} &= -P_{18}(1+\cos\theta_u)-P_{19}(1-\cos\theta_u)-P_5\sin\theta_u/4 \\ &+\frac{[\sin\frac{1}{2}\theta_l(P_7\sin\frac{1}{2}\theta_u+4P_{16}\cos\frac{1}{2}\theta_u)+\cos\frac{1}{2}\theta_l(P_6\cos\frac{1}{2}\theta_u+4P_{17}\sin\frac{1}{2}\theta_u)]^2}{[A+B+(A-B)/\cos\theta_u]-[D+C+(D-C)/\cos\theta_l]} \\ &+\frac{[\cos\frac{1}{2}\theta_l(P_7\sin\frac{1}{2}\theta_u+4P_{16}\cos\frac{1}{2}\theta_u)-\sin\frac{1}{2}\theta_l(P_6\cos\frac{1}{2}\theta_u+4P_{17}\sin\frac{1}{2}\theta_u)]^2}{[A+B+(A-B)/\cos\theta_u]-[D+C-(D-C)/\cos\theta_l]},\end{aligned} \tag{30}$$

where a_0 is the *conventional* unit cell lattice constant (i.e., $a_0=5.65$ Å for GaAs), $A-D$ remain defined by Eqs. (7) and (8), and the angles θ_u and θ_l are defined by

$$\cos\theta_u\equiv\frac{A-B}{\sqrt{(A-B)^2+4P_5^2}},\quad \sin\theta_u\equiv\frac{2P_5}{\sqrt{(A-B)^2+4P_5^2}}, \tag{31}$$

$$\cos\theta_l\equiv\frac{D-C}{\sqrt{(D-C)^2+4P_8^2}},\quad \sin\theta_l\equiv\frac{2P_8}{\sqrt{(D-C)^2+4P_8^2}}. \tag{32}$$

We should emphasize that Eq. (30) is valid for *all* choices of P_1-P_{23}; the variables $A-D$ are merely abbreviations. If we actually choose $A-D$ in accordance with Eqs. (14) and (15), then we can simplify Eq. (30) further by replacing the denominators of the second and third terms with $2[E(\Gamma_{1c})-E(\Gamma_{15c})]$ and $2[E(\Gamma_{1c})-E(\Gamma_{15v})]$, respectively. Note that the mass depends on P_{16} and P_{17} as well as the driving parameters P_5-P_8.

The dispersion relations for the $|p_{x0}\rangle$, $|p_{x1}\rangle$, $|p_{y0}\rangle$, and $|p_{y1}\rangle$ block, on the other hand, can be expressed in closed form for all k_z as

$$E(0,0,k_z)=\frac{A'+B'}{2}\pm\sqrt{\left(\frac{A'-B'}{2}\right)^2+C'^2+D'^2}, \tag{33}$$

with

$$A'=P_3+P_{14}[1+\cos(\tfrac{1}{2}k_z a_0)]+P_{10}\cos(\tfrac{1}{2}k_z a_0), \tag{34}$$

$$B'=P_4+P_{15}[1+\cos(\tfrac{1}{2}k_z a_0)]+P_{11}\cos(\tfrac{1}{2}k_z a_0), \tag{35}$$

$$C'=\sin(\tfrac{1}{4}k_z a_0)P_9, \tag{36}$$

$$D'=\cos(\tfrac{1}{4}k_z a_0)P_8. \tag{37}$$

Differentiating Eq. (33) twice with respect to k_z and taking the appropriate root gives the valence-band mass, and when we substitute Eqs. (14)–(29) we obtain the remarkably simple expression

$$\begin{aligned}\frac{4\hbar^2}{a_0^2 m_{\rm hh}^{(001)}} &= [E(\Gamma_{15v})-\Sigma X_5]/2+[P_8^2+P_9^2 \\ &+2\sqrt{(\Delta\Gamma_{15}^2-P_8^2)(\Delta X_5^2-P_9^2)}]/(4\Delta\Gamma_{15}).\end{aligned} \tag{38}$$

Therefore the (001) valence-band mass depends *only* on P_8, P_9, and the critical point energies, provided that all supplemental constraints (14)–(29) are followed. Solving Eq. (38) for P_9 in terms of P_8 gives

$$P_9^2=\chi-2\Delta\Gamma_{15}^2+P_8^2-2\sqrt{(\Delta\Gamma_{15}^2+\Delta X_5^2-\chi)(\Delta\Gamma_{15}^2-P_8^2)}, \tag{39}$$

where

TABLE I. Optimized tight-binding parameters.

Parameter	GaAs	GaSb	AlAs	InAs	InSb
P_1	−9.081 91	−8.828 99	−7.649 84	−9.531 58	−8.732 26
P_2	−2.376 29	−3.408 29	−1.094 55	−3.662 47	−3.590 52
P_3	−1.374 69	−0.695 70	−0.699 42	−0.444 92	−0.490 99
P_4	7.123 85	5.422 82	6.866 14	6.036 27	4.644 59
P_5	−6.146 27	−5.537 07	−6.138 97	−5.731 23	−4.869 33
P_6	2.794 74	2.289 51	4.391 86	2.662 04	2.530 17
P_7	4.624 75	4.082 26	4.083 82	4.240 65	3.751 28
P_8	−0.225 82	−0.565 43	−0.223 38	−0.110 24	−0.337 89
P_9	4.129 59	4.268 07	4.241 85	4.229 98	3.921 00
P_{10}	0.365 47	0.133 28	−0.087 32	0.405 13	0.221 90
P_{11}	−4.149 31	−3.054 16	−4.451 75	−2.940 78	−2.430 31
P_{12}	0.680 23	0.148 41	0.739 56	0.034 67	−0.063 08
P_{13}	−2.244 39	−1.590 53	−2.498 47	−1.271 02	−0.875 52
P_{14}	0.510 13	0.326 70	0.396 70	0.021 24	0.151 63
P_{15}	0.822 21	0.572 68	1.071 97	0.705 91	0.563 27
P_{16}	−1.442 01	−1.216 11	−1.711 45	−1.044 03	−0.950 95
P_{17}	0.509 43	0.344 65	0.932 94	0.087 24	0.374 90
P_{18}	0.048 23	0.004 30	−0.223 94	0.072 10	−0.154 54
P_{19}	0.094 24	0.345 89	0.244 08	0.235 25	0.437 13
P_{20}	0.054 94	0.232 71	1.279 61	0.192 87	0.563 23
P_{21}	0.697 42	0.461 70	−0.822 16	0.473 85	0.109 71
P_{22}	0	0	0	0	0
P_{23}	0	0	0	0	0

$$\chi \equiv 2\Delta\Gamma_{15}\left[\Sigma X_5 - E(\Gamma_{15v}) + \frac{8\hbar^2}{a_0^2 m_{\rm hh}^{(001)}}\right]. \qquad (40)$$

We choose $P_9>0$ in accordance with two-center binding arguments.

III. RESULTS

Evaluating P_1-P_4, $P_{10}-P_{15}$, P_{18}, and P_{19} in accordance with Eqs. (14)–(19) and (24)–(29) constrains the band structure to fit $E(L_{3v})$, $E(L_{3c})$, and all of the Γ and X energies exactly; fixing P_9 with Eq. (39) forces the exact heavy-hole

TABLE II. Resulting critical point energies (measured in eV) and masses (measured in m_0); m_c and $m_{\rm hh}$ result from the parameters in Table I while m_c[a] and $m_{\rm hh}$[a] result from the parameters in Ref. 11.

	GaAs	GaSb	AlAs	InAs	InSb
$E(\Gamma_{1v})$	−12.550	−12.000	−11.658	−12.690	−11.710
$E(\Gamma_{15v})$	0.000	0.000	−0.004	0.000	0.000
$E(\Gamma_{1c})$	1.519	0.813	2.974	0.418	0.235
$E(\Gamma_{15c})$	4.630	3.605	4.569	4.390	3.375
$E(X_{1v})$	−9.830	−9.330	−9.417	−10.200	−9.200
$E(X_{3v})$	−6.880	−6.760	−5.545	−6.640	−6.430
$E(X_{5v})$	−2.940	−2.490	−1.967	−2.470	−2.345
$E(X_{1c})$	2.030	1.720	2.262	2.280	1.710
$E(X_{3c})$	2.380	1.790	2.626	2.660	1.830
$E(X_{5c})$	12.473	10.138	12.672	10.547	8.707
$E(L_{1v})$	−10.600	−10.170	−10.075	−10.920	−9.950
$E(L_{2v})$	−6.830	−6.250	−5.529	−6.230	−5.920
$E(L_{3v})$	−1.310	−1.225	−0.749	−1.260	−1.200
$E(L_{1c})$	1.820	1.220	2.756	1.530	1.030
$E(L_{3c})$	5.495	4.510	5.157	5.420	4.415
m_c	0.067	0.042	0.154	0.022	0.0137
$m_{\rm hh}$	0.353	0.286	0.422	0.345	0.278
m_c[a]	0.214	0.089	1.172	0.037	0.0264
$m_{\rm hh}$[a]	0.341	0.235	0.563	0.338	0.208

[a]Reference 11.

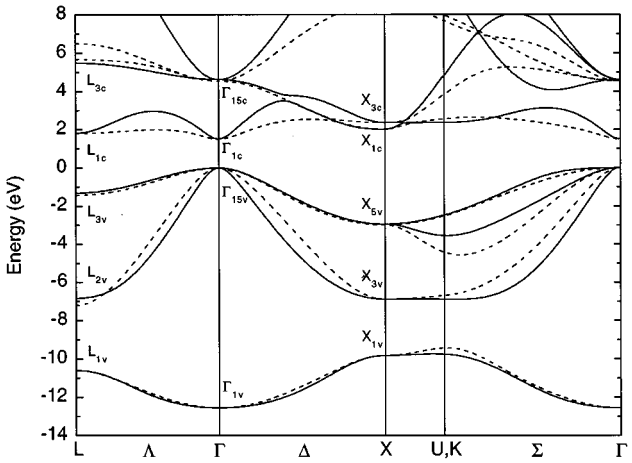

FIG. 1. GaAs band structure.

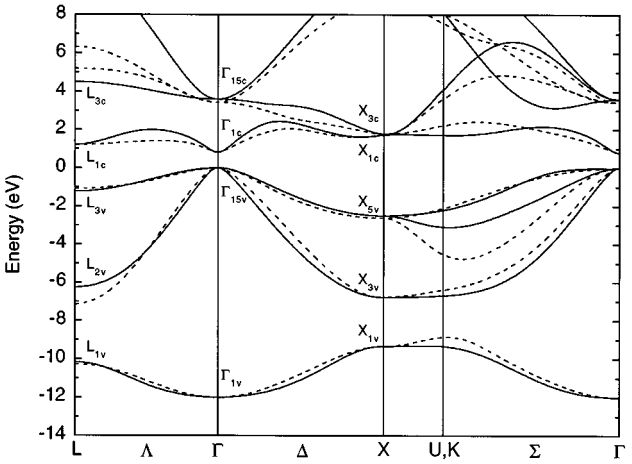

FIG. 2. GaSb band structure.

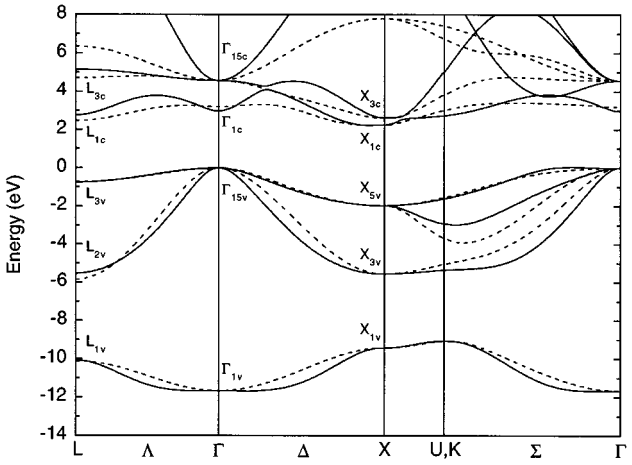

FIG. 3. AlAs band structure.

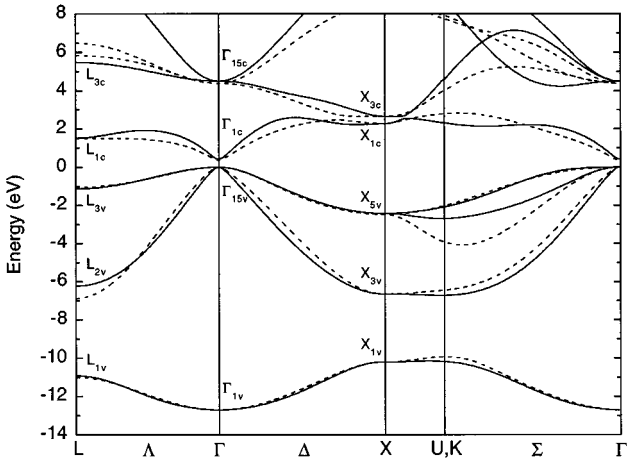

FIG. 4. InAs band structure.

mass. Since P_{22} and P_{23} do not appear in any constraint equations we set them both to zero, leaving us with eight independent parameters—P_5-P_8, P_{16}, P_{17}, P_{20}, and P_{21}—that we vary to fit $E(L_{1v})$, $E(L_{2v})$, $E(L_{1c})$, and the conduction-band effective mass.[12] [We were unable to fit $E(L_{2c})$: forcing its correct value distorted the bands.] For GaAs, GaSb, InAs, and InSb this approach worked quite well, and we fit the conduction-band masses to within $0.001m_0$ and the nonanalytic L-point energies to within 0.1 meV.[13] For AlAs, unfortunately, this fitting scheme always produced an offset valence-band maximum along the Σ direction that was $\sim$100 meV above the Γ-point value. By relaxing our constraints, and incurring $\sim$10 meV errors at the critical points, we reduced the undesirable maximum to $\sim$50 meV. Although this offset valence band makes our parameter set unsuitable for (011) AlAs valence-band calculations, the $Al_{0.30}Ga_{0.70}As$ bands, more relevant for heterostructure calculations, are valid. All parameters, energy gaps, and effective masses are presented in Tables I and II, and the band structures obtained from our new parameters (solid lines) and the original parameters (dotted lines, from Ref. 11) are shown in Figs. 1–5. Clearly the new parameter set gives much greater conduction-band curvature, while both sets are quite similar at Γ, X, and L. The K-point energy differences

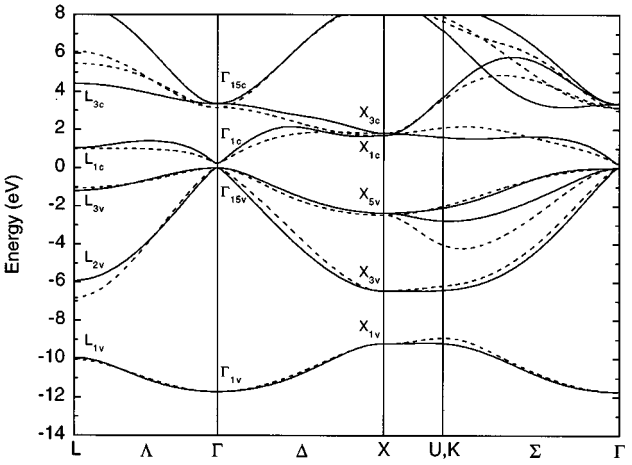

FIG. 5. InSb band structure.

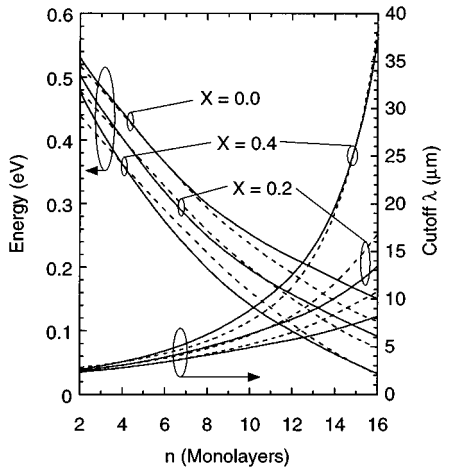

FIG. 6. Calculated band gaps E_g and cutoff wavelengths $\lambda=\hbar c/E_g$ of strained $(InAs)_n/(In_xGa_{1-x}Sb)_n$ superlattices grown on GaSb substrates. The solid lines use the parameters in Table I; the dotted lines use the parameters in Ref. 11.

result because the original parameter set was fitted pseudopotential calculations there, while the new parameters were not.

We have also illustrated the differences between the old and new parameters by incorporating both sets in energy band-gap calculations for strained $(InAs)_n/(In_xGa_{1-x}Sb)_n$ superlattices grown on GaSb substrates. The calculations are performed as described in Ref. 14, and we present results for the new parameters (solid lines) and the original parameters (dotted lines) in Fig. 6. As expected, the new parameter set gives substantially different results and agrees more closely with 8×8 $\mathbf{k}\cdot\mathbf{p}$ calculations, such as those reported in Refs. 14 and 15.

IV. CONCLUSION

By inverting the critical point energy constraints and fitting the effective masses we ensure more accurate bands near Γ and reduce the number of free tight-binding parameters from 23 to 8. These improvements let us calculate superlattice band gaps more accurately, but such *optical* properties can be calculated more easily within the $\mathbf{k}\cdot\mathbf{p}$ model since they are dominated by the *zone-center* band structure. The real advantages of the zinc-blende tight-binding model emerge when addressing full-zone effects, such as Γ to X tunneling, and full-band transport calculations[16,17] could benefit from our parameters in Table I. These parameters could be improved further by fitting the satellite valley near X to the measured effective mass. We could also improve the valence-band description by repeating the entire fitting procedure for the spin-dependent tight-binding model. Unfortunately, many of the critical point energies and effective masses cannot be obtained from the spin-dependent Hamiltonian in closed form, making them much more difficult to fit.

ACKNOWLEDGMENTS

The authors would like to thank B. Jogai for pseudopotential calculations of the X_{5c} critical point energies and R. E. Sherriff for a critical reading of the manuscript.

APPENDIX

Certain expressions in Ref. 11 should be corrected as follows:

$$\langle p_{x0}|p_{y0}\rangle=-4E_{xy}(110)_0S_1S_2-4iE_{xy}(011)_0S_3(C_1-C_2), \tag{A1}$$

$$\langle s_0|p_{z0}\rangle=-4E_{sx}(011)_0S_1S_2+4iE_{sx}(110)_0S_3(C_1+C_2), \tag{A2}$$

$$\langle s_1|p_{z0}\rangle=-4E_{sx}(0.5,0.5,0.5)_{10}g_3^*, \tag{A3}$$

$$\langle p_{x0}|p_{z0}\rangle=-4E_{xy}(110)_0S_1S_3-4iE_{xy}(011)_0S_2(C_1-C_3), \tag{A4}$$

$$\langle p_{y0}|p_{z0}\rangle=-4E_{xy}(110)_0S_2S_3-4iE_{xy}(011)_0S_1(C_2-C_3), \tag{A5}$$

$$\langle s_1|p_{x1}\rangle=4E_{sx}(011)_1S_2S_3+4iE_{sx}(110)_1S_1(C_2+C_3), \tag{A6}$$

$$\langle p_{x1}|p_{y1}\rangle=-4E_{xy}(110)_1S_1S_2+4iE_{xy}(011)_1S_3(C_1-C_2), \tag{A7}$$

$$\langle s_1|p_{z1}\rangle=4E_{sx}(011)_1S_1S_2+4iE_{sx}(110)_1S_3(C_1+C_2), \tag{A8}$$

$$\langle p_{x1}|p_{z1}\rangle=-4E_{xy}(110)_1S_1S_3+4iE_{xy}(011)_1S_2(C_1-C_3), \tag{A9}$$

$$\langle p_{y1}|p_{z1}\rangle=-4E_{xy}(110)_1S_2S_3+4iE_{xy}(011)_1S_1(C_2-C_3), \tag{A10}$$

$$g_0=\cos(\pi k_x/2)\cos(\pi k_y/2)\cos(\pi k_z/2) - i\,\sin(\pi k_x/2)\sin(\pi k_y/2)\sin(\pi k_z/2), \tag{A11}$$

$$E(\Gamma_{15c})=\left[\frac{C+D}{2}\right]+\left\{\left[\frac{C-D}{2}\right]^2+P_8^2\right\}^{1/2}, \tag{A12}$$

$$E(\Gamma_{15v})=\left[\frac{C+D}{2}\right]-\left\{\left[\frac{C-D}{2}\right]^2+P_8^2\right\}^{1/2}. \tag{A13}$$

Note that in Ref. 11, and hence in this appendix, $\mathbf{k}$ is *implicitly* measured in units of $2\pi/a_0$, where a_0 is the *conventional* unit cell lattice constant (i.e., $a_0=5.65$ Å for GaAs). In the rest of this paper we measure $\mathbf{k}$ in angstroms and *explicitly* denote any a_0 dependence.

[1] J. C. Slater and G. F. Koster, Phys. Rev. **94**, 1498 (1954).
[2] D. J. Chadi and M. L. Cohen, Phys. Status Solidi B **68**, 405 (1975).
[3] P. Vogl, H. P. Hjalmarson, and J. D. Dow, J. Phys. Chem. Solids **44**, 365 (1983).
[4] E. O. Kane, in *Physics of III–V Compounds*, edited by R. K. Willardson and A. C. Beer, Semiconductors and Semimetals Vol. 1 (Academic, New York, 1966), p. 75.
[5] J. M. Luttinger and W. Kohn, Phys. Rev. **97**, 869 (1955).
[6] J. N. Schulman and T. C. McGill, Phys. Rev. Lett. **39**, 1680 (1977).
[7] J. N. Schulman and Y. C. Chang, Phys. Rev. B **31**, 2056 (1985).
[8] G. Bastard and J. A. Brum, IEEE J. Quantum Electron. **22**, 1625 (1986).
[9] D. Ahn, S. L. Chuang, and Y. C. Chang, J. Appl. Phys. **64**, 4056 (1988).
[10] Reference 7 is a notable exception.
[11] D. N. Talwar and C. S. Ting, Phys. Rev. B **25**, 2660 (1982).
[12] We used the AMOEBA routine found in W. H. Press, S. A. Teukolsky, W. T. Vetterling, and B. P. Flannery, *Numerical Recipes* (Cambridge University Press, New York, 1992), to perform a numerical search for the best parameters.
[13] For GaAs, GaSb, InAs, and InSb we fit the spin-averaged pseudopotential results in J. R. Chelikowsky and M. L. Cohen, Phys. Rev. B **14**, 556 (1976); for AlAs we fit the energy values in E. Hess, I. Topol, K. R. Schülze, H. Neumann, and K. Unger, Phys. Status Solidi B **55**, 187 (1973).
[14] D. N. Talwar, J. P. Loehr, and B. Jogai, Phys. Rev. B **49**, 10 345 (1994).
[15] C. Mailhiot and D. L. Smith, J. Vac. Sci. Technol. B **5**, 1268 (1987).
[16] D. Z.-Y. Ting, E. T. Yu, and T. C. McGill, Phys. Rev. B **45**, 3583 (1992).
[17] R. C. Bowen, W. R. Frensley, G. Klimeck, and R. K. Lake, Phys. Rev. B **52**, 2754 (1995).